Vibrational and Rotational Cooling of H_3^+

H. Kreckel,[1] S. Krohn,[1] L. Lammich,[1] M. Lange,[1] J. Levin,[1] M. Scheffel,[1] D. Schwalm,[1] J. Tennyson,[3] Z. Vager,[2] R. Wester,[1] A. Wolf,[1] and D. Zajfman[2]

[1] *Max-Planck-Institut für Kernphysik, 69117 Heidelberg, Germany*
[2] *Weizmann Institute of Science, 76100 Rehovot, Israel*
[3] *Department of Physics and Astronomy, University College London, London WC1E 6BT, UK*

(Dated: July 22, 2002 — To be submitted to Phys. Rev. A)

The vibrational relaxation of H_3^+ molecules from a conventional plasma ion source is studied performing Coulomb explosion imaging on the ions extracted from a storage ring after variable times of storage. Storage for 2 s is found sufficient for radiative relaxation of the breathing excitation and the fragment velocity distribution in the breathing coordinate then agrees well with simulations based on the calculated ground-state wave function. The radiative decay of the two lowest pure breathing levels $(1,0^0)$ and $(2,0^0)$ is seen to be considerably faster than expected from rotationless calculations. Assuming a high rotational excitation of the H_3^+ ions, as suggested already in earlier experiments, the theoretical transition probabilities of the UCL line list for H_3^+ [L. Neale, S. Miller and J. Tennyson, Astrophys. J. **464**, 516 (1996)] can explain the increase of the vibrational cooling rates and reproduce the observed decay curve for the lowest breathing-excited level, confirming the absolute transition probabilities of these line tables. The observations give evidence for a quasi-stable population of high-lying rotational levels in the stored ion beam, relevant for the interpretation of storage ring measurements on the rate coefficients for dissociative recombination of H_3^+ ions with low-energy electrons.

PACS numbers: 33.15.-e, 34.80.Lx

I. INTRODUCTION

The H_3^+ ion is the most simple polyatomic molecule and therefore an attractive model system for high-precision quantum chemical calculations and for the basic understanding of interactions within molecules. A large variety of surprising and interesting dynamical features, as reviewed in [1, 2], are reflected in particular by the ro-vibrational absorption and emission spectra. Moreover, the electronic structure and its interplay with the nuclear motion, especially in the related instable neutral system H_3, continue to raise intriguing questions studied in close interaction between theory and experiments [3–5]. Much of the interest in the physics of H_3^+ is also based on its large abundance in cold ionized matter, from laboratory plasmas to the interstellar medium [6], and on its high reactivity, by which it initiates extensive reaction chains notably in interstellar chemistry [7, 8]. The long-predicted presence of H_3^+ in the interstellar medium could be confirmed only in recent years by the observation of infrared absorption spectra [9, 10].

The large abundance of H_3^+ in cold hydrogen plasmas arises from its efficient production by the process $H_2 + H_2^+ \rightarrow H_3^+ + H$, which is exothermic by as much as 1.7 eV and thus yields H_3^+ ions with large degrees of ro-vibrational excitation. In a cold, low-density environment such as the interstellar medium, the H_3^+ ions can cool radiatively before further interactions, giving up their ro-vibrational excitation energy by infrared emission. On the other hand, in laboratory investigations of H_3^+ and its interactions, special precautions are required to obtain results for ro-vibrationally relaxed ions. Among the processes which can be strongly influenced by the internal excitation of a molecular ion, the dissociative recombination (DR) with low-energy electrons is an important example. For H_3^+, this process is described by

$$H_3^+ + e^- \rightarrow \begin{cases} H(1s) + H(1s) + H(1s) \\ H_2(X^1\Sigma_g^+) + H(1s), \end{cases} \quad (1)$$

where the given electronic states are the only possible ones for initial energies of $\lesssim 1$ eV with respect to the ground state of H_3^+, and where the ratio of three-body to two-body fragmentation is found [11] to be $\sim$3. The DR rate coefficient has a strong influence on the H_3^+ abundance, and hence on all the reaction chains initiated by this ion, in theoretical models of the chemistry in the interstellar medium [12]. It has therefore been measured by many experiments using various techniques. The results scatter in a wide range ($<1 \times 10^{-10}$ to 2×10^{-7} $cm^3\,s^{-1}$ for a 300-K electron temperature), uncontrolled ro-vibrational excitation being considered as one of the possible reasons for these discrepancies [13]. Experiments using merged electron and ion beams, employing a magnetic storage ring to recirculate the ions at MeV laboratory energies, have been introduced more recently for DR measurements [14]. In addition to well controlled detection and normalization techniques, this arrangement

offers the possibility of storing the molecular ions for times up to minutes; for many species, this is clearly sufficient to achieve a complete relaxation of the internal molecular degrees of freedom, as ions produced in excited states can radiatively cool and thermalize with the ambient temperature of the storage ring. Several experimental tests demonstrating vibrational and also rotational relaxation of ions used in storage ring DR measurements have been performed [15, 16], confirming the expected radiative cooling for infrared active species. Rate coefficients for the DR of H_3^+ after several seconds of radiative cooling have been measured at the storage rings CRYRING [17], TARN II [18] and ASTRID [19], yielding values of $\sim 1 \times 10^{-7}$ cm^3 s^{-1} at 300 K which agree among each other within the experimental errors. Implications of the measured values and their comparison to theoretical predictions have been discussed in recent publications [20, 4, 3].

Regarding the radiative cooling of the ro-vibrational degrees of freedom, the situation of H_3^+ is less clear than for many other species as the high symmetry of this molecule leads to infrared-inactive vibrational and rotational modes, which, however, coexist with other infrared active modes so that 'forbidden' decays can become rather efficient. In the present work, we experimentally address the relaxation of excited H_3^+ molecules in the essentially collision-free environment of an ion storage ring. Using the Coulomb explosion imaging (CEI) method, we follow in time the degree of vibrational excitation found for H_3^+ ions produced in a standard plasma ion source and stored as a fast beam for several seconds. The observed time dependence of the vibrational excitation is compared with theoretically predicted ro-vibrational emission rates, and this comparison turns out to give indications also about the rotational excitation of the investigated molecules. Spontaneous radiative decay curves are measured explicitly for the first and second breathing excitations of H_3^+, and the extent to which ro-vibrational cooling of H_3^+ ions can be achieved by relying on radiative emission is analyzed on the basis of experimental and theoretical data.

The results show that complete relaxation can be achieved within $\sim$2 s for the vibrational degrees of freedom, including the infrared-inactive breathing mode. However, in the quantitative analysis theoretical ro-vibrational decay rates are found to reproduce the measured decay curves only if a high rotational excitation of the H_3^+ molecules is assumed. A ro-vibrational relaxation model constructed to reproduce the measured decay curves predicts an average rotational energy of about 0.3 eV even after storage times of up to 60 s. This energy value is consistent with those inferred from separate measurements at the same facility [21, 22] by analyzing the kinetic energy release in the DR process described by Eq. (1). Moreover, the good description of the measured time dependence of the population of the first breathing level by our model calculation gives an experimental confirmation of the theoretically predicted absolute radiative decay rates for H_3^+.

II. EXPERIMENTAL METHOD AND SETUP

In the CEI method [23], fast molecular ions with a velocity of several atomic units (a.u.) are directed towards a very thin foil (thickness <100 Å) where their binding electrons are stripped off within 10^{-16} s. This time, as well as the dwell time in the foil of $\sim 10^{-15}$ s, is much shorter than the vibrational and rotational time scales (10^{-14} s and 10^{-12} s, respectively) so that the nuclear geometry of the molecular ion is left unchanged during the stripping process. The positively charged atomic fragments resulting from the stripping process repel each other, largely after having left the foil, reaching asymptotic velocities after flight times of the order of $\sim 10^{-14}$ s. The asymptotic velocities are read out from the spatial arrangement of the fragments after a drift distance of a few meters, using position and time sensitive multiparticle imaging detectors. The asymptotic velocities determined in a CEI experiment carry information about the positions of the individual nuclei in the molecule at the time of the stripping process; for an ensemble of events, this corresponds to the distribution of nuclear coordinates as described by the quantum mechanical probability density, i.e., the square of the nuclear wave function. For the interpretation of CEI data, the asymptotic velocity distributions are usually forward-simulated starting from given quantum mechanical probability densities; alternatively, spatial density distributions of the nuclei in the molecule can be reconstructed from CEI data using suitable inversion methods.

The asymptotic velocity distributions observed by CEI or the reconstructed spatial density distributions reflect not only the ground-state geometry, but also the degree of internal excitation of the investigated molecular ions. In particular, a vibrational excitation directly modifies the observed distributions, reflecting the different shapes of the probability density for excited quantum levels and their relative contributions. Therefore, applied to ions previously stored in a low-perturbation environment for variable times, the CEI method can be used to study vibrational relaxation processes as induced by spontaneous radiative emission. Ion storage rings provide such an environment for fast ion beams, and CEI at a heavy ion storage ring has recently been used by us to analyze the initial excitation and radiative relaxation of stored HD^+ ions [24]; similarly, we have recently studied vibrational excitation by slow electron collisions on the diatomic hydrogen molecular ions H_2^+ [25] and D_2^+.

Our experiments are carried out using the heavy-ion Test Storage Ring (TSR), located at the Max-Planck-Institut für Kernphysik, Heidelberg, together with the CEI setup installed at this facilty [26]. H_3^+ molecular ions were produced in a 'hot' gas discharge ion source and accelerated by a radio-frequency quadrupole accelerator to $v_0 = 0.032\,c$ ($\sim$4.4 a.u.), corresponding to a kinetic energy of 1.43 MeV. The ions are injected into the storage ring and accumulated there during a time of

$\sim$30 μs, yielding about 10^6 ions which then circulate in the ring (55.4 m circumference) in an average vacuum of $\sim 3 \times 10^{-11}$ mbar for storage times of the order of 10 s. The ion velocity in the magnetic storage ring remains unchanged from that after the initial acceleration and is known within a relative error of $\pm 3.5 \times 10^{-3}$; the relative velocity spread is well below 1×10^{-3}. While the ions are stored, a 'slow extraction' mode [26] can be activated which continuously peels off a small part of them from the circulating beam; these extracted ions (typical rate 10^3 s^{-1}) are guided towards the CEI setup through an external beamline. The extraction takes place at the same storage ring position as the injection; by changing the deflecting fields at this ring element, the ions can also be transferred directly into the extraction beamline, bypassing the storage ring.

After collimation to an angular spread of $\lesssim 0.3$ mrad and a spot size of $\sim$0.5 mm diam. the H_3^+ ions hit a diamond-like carbon (DLC) target [27] with a thickness of 0.7 μg/cm^2. The protons originating from the Coulomb explosion in the foil target reach typical distances of $\sim$50 mm after a drift distance of $L = 4616 \pm 4$ mm, where they impinge on a multi-hit three-dimensional (3D) imaging detector oriented vertical to the ions' center-of-mass motion. The drift distance was increased by $\sim$1.5 m with respect to our earlier CEI experiments in order to optimize the resolution of the measured asymptotic velocity distributions. The 3D imaging detector uses a multichannel plate (MCP) equipped with a phosphorescent anode; for single-molecule events, the fragment impact positions in the detector plane are read out by recording an image of the light flashes on the anode by a CCD camera, while the longitudinal distances between the fragments on arriving at the detector are derived from the time differences between the fragment impacts, read out electronically using a system of strip electrodes integrated in the anode; details about this imaging detector are given in Ref. [26]. The fragment hit times were measured with a root-mean-square (r.m.s.) spread of 100 ps at typical time differences of $\sim$5 ns. As compared to the initial arrangement [26] the present experiments employ an improved pre-amplifier system which was developed on the basis of detailed test measurements on the multihit timing performance, using UV-laser double pulses with adjustable nanosecond time delays [28].

Coulomb explosion events of extracted H_3^+ ions are recorded on a single molecule basis, letting the first counting pulse seen at the CEI detector trigger a beam deflector on the extraction line that blocks the access to the CEI setup for all following ions. Typically 20 ms later the CEI detector is ready to record the next event and extracted molecules are admitted again to the CEI setup. Together with the imaging data also the arrival time of the molecule is recorded, measured with respect to the injection time of the H_3^+ ion beam into the storage ring. Collecting data for many subsequent injection and slow-extraction cycles, asymptotic velocity distributions can be built up for time slices representing the delay since the H_3^+ ions left the ion source. After $\sim$2 h of total run time, typically 140000 fully analyzed events were obtained in single 1-ms wide storage time bins. The earliest time bin was for storage times of 2–3 ms and the storage times were extended up to 6 s. In addition, CEI data were also taken for the direct H_3^+ beam, bypassing the storage ring as described above. For these events, the delay since the H_3^+ ions left the ion source amounts to $\sim$10 μs, corresponding to the length of $\sim$100 m over which the ions are transported.

III. BREATHING-MODE RELAXATION MEASUREMENTS

A Vibrational excitation of H_3^+

The equilibrium geometry of the nuclei in H_3^+ is an equilateral triangle with a predicted bond length of 0.873 Å. Excursions from the equilibrium are described using the normal coordinates (adapted to the C_{3v} symmetry group of the planar triangular geometry) defined by

$$s_a = (r_{12} + r_{23} + r_{31})/\sqrt{3} \tag{2}$$

for the symmetric stretch or 'breathing' mode conserving the equilateral symmetry and by

$$s_x = (2\,r_{12} - r_{23} - r_{31})/\sqrt{6}, \tag{3}$$

$$s_y = (r_{23} - r_{31})/\sqrt{2} \tag{4}$$

for the deformations changing the triangular shape, causing two modes of bending vibrations degenerate in the harmonic approximation. Here, r_{ij} denotes the distance between any two nuclei i and j. In the harmonic approximation, the breathing and bending vibration frequencies are $\nu_1 \sim 3200$ cm^{-1} and $\nu_2 \sim 2500$ cm^{-1}. Breathing excitations are labeled by the quantum number v_1 and bending excitations by $v_2^{|\ell|}$, including the vibrational angular momentum ℓ associated with the two degenerate bending modes. An overview of the scheme of low-lying vibrational levels is given in Ref. [2].

As the bending deformations are associated with a dipole moment, the ν_2 mode is infrared-active and the rates of the most favoured transitions involving changes of the v_2 quantum number are calculated [29] to be in the range of 100–150 s^{-1}, leading to radiative lifetimes of levels with $v_2 > 0$ in the range of < 10 ms. On the other hand, the breathing vibration is infrared inactive and levels with $v_1 > 0$ and $v_2 = 0$ are metastable with much longer radiative lifetimes. The dominant radiative decay occurs via mode-mixing overtone transitions; denoting the vibrationally excited levels by $(v_1, v_2^{|\ell|})$, the decay $(1, 0^0) \rightarrow (0, 1^1)$ with a calculated rate of 0.85 s^{-1} [29] leads to a predicted radiative lifetime of 1.18 s for the first metastable level $(1, 0^0)$. Similarly, the decays of the second metastable level $(2, 0^0)$ to mainly the $(1, 1^1)$ but

also to the $(0,1^1)$ and $(0,2^2)$ states using the rates from Ref. [29] lead to a prediction of 0.38 s for its radiative lifetime. These lifetimes have been derived in a rotationless approximation. Theoretical decay rates of individual assigned ro-vibrational levels (apart from levels the vibrational ground state [30]) so far are not directly accessible in the literature, although the relevant information can be combined from different sources, as discussed below (Sec. IV). As a general trend, the ro-vibrational calculations show a significant influence of rotational excitation on the vibrational relaxation rates due to radiative emission, which should be kept in mind in comparing experimental relaxation time constants to the rotationless lifetimes given above. Within the vibrational ground state the radiative decay of pure rotational excitation generally occurs at considerably smaller rates ($\lesssim 10^{-2}$ s^{-1}) by forbidden rotational transitions [30].

B Data representation and modeling

The CEI measurement yields the three asymptotic velocity vectors of the fragments in the center of mass frame of the dissociating molecule by evaluating the recorded event data. Conversion factors used to obtain the fragment velocities from the transverse positions and the time differences are v_0/L and v_0^2/L, respectively, where v_0 denotes the beam velocity and L the drift distance from the target foil to the detector. The size and the shape of the triangle spanned by the velocity vectors can be characterised by velocity coordinates adapted to the molecular symmetry defined similar to Eqs. (2)–(4),

$$v_a = (v_{12} + v_{23} + v_{31})/\sqrt{3}, \tag{5}$$

$$v_x = (2\,v_{12} - v_{23} - v_{31})/\sqrt{6}, \tag{6}$$

$$v_y = (v_{23} - v_{31})/\sqrt{2}, \tag{7}$$

where $v_{ij} = |\vec{V}_i - \vec{V}_j|$; the velocity of fragment i in the center of mass frame is denoted by $\vec{V}_i$. In addition, also the overall spatial orientation of the velocity triangle can be obtained from the data. Distributions of the events along the velocity coordinate v_a automatically fulfill the required invariance with respect to the exchange of fragments; on the other hand, distributions in v_x and v_y must be exchange-symmetrized in order to become independent of any arbitrary numbering of hits introduced during the event recording.

Basically, the size of the symmetric v_a coordinate is related to the average bond length of the three protons in the H_3^+ molecule [cf. Eq. (2)], while the asymmetric coordinates $v_{x,y}$ reflect the deformations from the equilateral geometry as expressed by $s_{x,y}$. In order to interpret the experimental results, measured asymptotic velocity distributions are modeled by a Monte Carlo simulation [31]. Initial molecular geometries are generated randomly according to a given quantum mechanical probability density (vibrational wave function), with a random overall orientation in space, and then propagated through the target foil simulating the stripping process as well as multiple scattering and charge exchange processes. After finding the asymptotic fragment velocities behind the foil, also details of the detector arrangement are simulated, such as finite time and position resolution, detection efficiencies, and possible cuts on the event data as applied in the analysis.

Rotationless ($J = 0$) wavefunctions for H_3^+ were calculated using program DVR3D [32]. The potentials and non-adiabatic corrections used are those of Polyansky and Tennyson [33], where further details of the calculation can be found. Simulations were performed for the lowest vibrational levels with breathing (ν_1) and bending (ν_2) excitation. According to the lifetimes discussed in Sec. III A, only the lowest breathing levels $(v_1, 0^0)$ will survive after the first ~50 ms of storage time. Excitation of this mode is found to affect almost exclusively the symmetric molecular coordinate s_a and hence the corresponding asymptotic velocity v_a. Simulated v_a distributions for levels with $v_1 \leq 2$ are shown in Fig. 1(a); they closely reflect the nodal structure and the increasing width of the spatial molecular wave functions, so that the observation of this asymptotic velocity coordinate is well suited for monitoring the breathing-mode relaxation. Simulated v_x and v_y distributions, which are predominantly sensitive to the bending vibrations, are displayed in Fig. 1(b) for levels with $v_2 \leq 1$. Note that for small vibrational quantum numbers the v_a ($v_{x,y}$) distributions are rather insensitive to bending (breathing) excitations. In fact, the v_a distribution for, e.g., the $(0,1^1)$ and $(1,1^1)$ excitations are indistinguishable within the drawing resolution of Fig. 1 from those for the $(0,0^0)$ and $(1,0^0)$ state, respectively. The simulations account for the experimental target thickness, which was determined by measuring the multiple scattering of atomic (H^+) ions on the same foil as used for the CEI measurements, deriving a value of $0.7 \pm 0.1\,\mu$g/cm^{-2}. As compared to the width caused by the initial spatial distribution of the nuclei in the molecule, multiple scattering broadens the observed asymptotic velocity distributions by ~20% for the present experimental parameters; it represents the dominant instrumental broadening.

The Monte Carlo simulation procedure used here was found to reproduce with good accuracy the asymptotic velocity distributions measured in previous CEI experiments on simple species with well-known molecular structure [26]. It does not include the effect of wake fields which the charged fragments induce by polarizing the electrons in the target foil. These fields can lead to distortions of the Coulomb explosion trajectories, which can be identified experimentally by studying the influence of the molecular orientation (as measured by the CEI detector) on the asymptotic velocity distributions. For planar molecules such as H_3^+ the wake effect can be minimized by selecting events for which the normal vector of the molecular plane at the starting time of the Coulomb explosion process is parallel to the center-of-mass velocity

vector within a small limiting angle θ.

In the present modeling procedure, the motion of the nuclei in the Coulomb explosion is treated classically after setting the starting positions in the molecular center of mass frame, and the initial velocities of the nuclei in this frame are neglected. The main reason for using this approximation is that the initial velocities can be included consistently only within a quantum mechanical treatment of the Coulomb explosion process, which is not yet available for the polyatomic system studied here. We can estimate the influence of this approximation on the centroid and the r.m.s. width of the v_κ distributions ($\kappa = a, x, y$) within the following simplifying classical approach: For the most likely spatial conformation of the H_3^+ ion in its vibrational ground state the individual protons i ($i = 1, 2, 3$) of mass m are accelerated in the Coulomb explosion along straight lines in the molecular c.m. system, aquiring final velocities of $|\vec{V}_i| = V_0 \sim 0.025$ a.u. (where 3.0 a.u. is used for the most likely value of the symmetric normal coordinate s_a as calculated from the ground-state wave function). The corresponding total kinetic energy is $E_0 = (3/2)\, mV_0^2 = 47$ eV, and the resulting mean asymptotic velocity expressed by the symmetric coordinate is $\langle v_a \rangle = 3V_0 = 0.075$ a.u. In this fully symmetric explosion geometry, a small initial velocity component $\hat{V}_{i\|}$ of a proton parallel to the acceleration direction leads to a change of the asymptotic velocity by $\delta V_{i\|} \simeq (1/2)V_0\, (\hat{V}_{i\|}/V_0)^2$; contrary, an initial velocity component $\hat{V}_{i\perp}$ perpendicular to this direction leads to $\delta V_{i\perp} = V_0\, (\hat{V}_{i\perp}/V_0)$. Setting the mean kinetic energy $(3/2)\, m\langle \hat{V}_\kappa^2 \rangle$ stored in the vibrational mode κ equal to half the zero point energy $(1/2)h\nu_\kappa$, and considering a Gaussian distribution of the initial velocities, it is straightforward to show that for the v_a distribution the shift $\langle \delta v_a \rangle_\kappa$ of the centroid and the r.m.s. width $\sigma_{a,\kappa}$ caused by the zero point motion in this mode are both of the same order of magnitude given by

$$\langle \delta v_a \rangle_\kappa \sim \sigma_{a,\kappa} \sim (1/2)\, \langle v_a \rangle\, h\nu_\kappa / 4E_0. \qquad (8)$$

Taking into account all three vibrational degrees of freedoms, a more detailed calculation results in a shift due to the zero point motion of $\langle \delta v_a \rangle_{\mathrm{ZPM}} = \sum_\kappa \langle \delta v_a \rangle_\kappa \sim 1.5 \times 10^{-4}$ a.u. and in an additional r.m.s. width of $\sigma_{a,\mathrm{ZPM}} = (\sum_\kappa \sigma_{a,\kappa}^2)^{1/2} \sim 1.1 \times 10^{-4}$ a.u. The given shift $\langle \delta v_a \rangle_{\mathrm{ZPM}}$ is very small compared to the mean asymptotic velocity $\langle v_a \rangle$ and also to the velocity width of $\sigma_{a,\mathrm{no\,ZPM}} = 3.4 \times 10^{-3}$ a.u. which results from the spatial distribution of the nuclei in the molecule before explosion [cf. Fig. 1(a)]. The same is true for the given additional r.m.s. width $\sigma_{a,\mathrm{ZPM}}$ which, moreover, has to be added in square to $\sigma_{a,\mathrm{no\,ZPM}}$. The situation is different for the $v_{x,y}$ distributions. While, after the symmetrization procedure discussed above, we have $\langle \delta v_{x,y} \rangle_{\mathrm{ZPM}} = 0$, the r.m.s. widths $\sigma_{x,\kappa}$ and $\sigma_{y,\kappa}$ caused by the initial velocities due to zero point motion in the modes $\kappa = x, y$ are considerably larger, as their order of magnitude is determined by

$$\sigma_{x,\kappa} \sim \sigma_{y,\kappa} \sim \langle v_a \rangle\, (h\nu_\kappa / 4E_0)^{1/2}. \qquad (9)$$

Performing the estimation in more detail and including the total zero point motion one obtains $\sigma_{x,\mathrm{ZPM}} \sim \sigma_{y,\mathrm{ZPM}} \sim 1.3 \times 10^{-3}$ a.u. which is of the same order as the velocity width resulting from the spatial distribution of the nuclei before the Coulomb explosion, amounting to $\sigma_{x,y,\mathrm{no\,ZPM}} \sim 3.5 \times 10^{-3}$ a.u.

From this argument, the present modeling procedure of the Coulomb explosion seems adequate for the breathing coordinate (v_a) but not for the bending coordinates ($v_{x,y}$). Because of the small influence of the initial velocities on the v_a distribution, the Monte-Carlo model remains adequate in this coordinate also for the low-lying excited vibrational levels of H_3^+. Regarding the influence of rotations, it can be shown by a similar classical estimate that even rotational energies of the order of several tenths of an eV have a negligible influence on the asymptotic velocity distributions after Coulomb explosion. It should be noted that in previous work on the vibrational excitation of HD^+ [24, 15] and H_2^+ [25] the initial velocities were included in the simulation by a procedure [15] adapted specially to the diatomic species treated there.

C Results

The measured asymptotic velocity distributions in characteristic stages of the relaxation process are shown in Fig. 2. Data for the H_3^+ beam arriving directly from the accelerator are compared to those obtained after storage in the ring for times of 30–50 ms and of > 2 s. Values for the v_a coordinate are concentrated in a narrow range around 0.075 a.u. The v_a distribution shifts upwards and narrows down by the storage of the H_3^+ ions, as expected for a temporal decrease of contributions from breathing-excited levels according to Fig. 1(a). A stable shape of the distribution is reached for > 2 s of storage. The distributions in v_x and v_y (centered around zero by symmetry) also narrow down by the ion storage; however, they reach an essentially stable shape already after ~50 ms. This relaxation behaviour qualitatively agrees with the radiative emission properties of the infrared-inactive breathing mode (reflected by the v_a coordinate) and the infrared-active bending modes ($v_{x,y}$ coordinates) as discussed in Sec. III A.

Note that for the velocity distributions shown in Fig. 2 and those discussed further below, as well as for all quantities deduced from them (with the exception of Figs. 3 and 4 where the full data sets have been used), the molecular orientation angle θ (see Sec. III B) was chosen to be $|\cos\theta| > 0.8$ to minimize possible distortions by wake effects. In fact, considering all orientation angles instead of only those with $|\cos\theta| > 0.8$, a shift (broadening) of +0.4% (−7%) was found (and attributed to wake effects) in the v_a distribution recorded after a storage time of 2 s;

on the other hand, when the θ cut was even further restricted no further statistical significant changes of the v_a or the $v_{x,y}$ distributions were observed.

More detailed information about the relaxation process can be obtained in a first approach by considering the r.m.s. widths of the asymptotic velocity distributions as a function of time. Disregarding at this stage the exact functional shape of the distributions and (storage time independent) wake effects by allowing for all orientation angles θ, we have determined for various time slices the r.m.s. deviations of the measured probability densities from the mean values. For the v_a coordinate the results are displayed in Fig. 3. The time dependence can be well represented by fitting the sum of three exponential functions plus a constant. A slow component with a time constant of 500±60 ms describes the cooling from a few hundred milliseconds up to ∼2 s. At shorter times, a faster component with a time constant of 53±6 ms is clearly distinguishable (see inset in Fig. 3). Additional decay components with even faster cooling occur only for very short storage times ($\lesssim$25 ms) and a third exponential component is introduced in the fit to describe the few data points available in this time range. It is tempting to assign the two clearly distinguished components with time constants of 500±60 ms and 53±6 ms to the decay of the two lowest metastable vibrational levels $(1,0^0)$ and $(2,0^0)$, the most long-lived levels among the excited vibrational states of H_3^+, as discussed in Sec. III A. However, the lifetimes predicted for these two levels in the rotationless approximation are larger than the observed time constants by factors of ∼2.6 for the $(1,0^0)$ level and even ∼8 for the $(2,0^0)$ level. For the coordinates v_x and v_y (see Fig. 4) the r.m.s. velocity width shows a very fast inititial decay with a time constant of <10 ms. This clearly reflects the fast relaxation of bending excitations. After ∼50 ms only a very small further decrease of the width is seen; this can be understood from the slight dependence of the $v_{x,y}$ distributions on the breathing excitation and the intermediate population of states with $v_2 > 0$ in the decay cascades of the $(v_1,0^0)$ excitations.

Although the vibrational relaxation of the stored H_3^+ ions can be clearly followed in the widths of the v_κ distributions as a function of time (Figs. 3, 4), and even time constants describing the relaxation can be extracted as demonstrated above, it still remains to derive quantitative information on the time dependences of the vibrational state populations. We have therefore performed a more elaborate analysis of the shapes of the measured v_κ distributions by fitting them with Monte-Carlo generated distributions (see Sec. III B). To investigate the quality of our Monte Carlo procedure we first compared the 'relaxed' distributions to the Monte-Carlo simulations obtained with the vibrational wavefunction of the $(0,0^0)$ ground state of H_3^+, both for the v_a and the $v_{x,y}$ coordinates. For the v_a coordinate [Fig. 5(a)] the simulation shows excellent agreement with the measured data. No adjustments in the simulation had to be or were done to fit the data. The observed agreement is a strong indication that the H_3^+ ions have essentially relaxed to the vibrational ground state after a storage time of 2 s. For the v_x and v_y coordinates, the measured distributions are ∼20% wider than the ground-state simulation. However, the discussion in Sec. III B has shown that the approximations used in modeling the Coulomb explosion are much less justified for the $v_{x,y}$ coordinates, which represent deformations perpendicular to the radial expansion of the molecule with respect to its center of mass. In fact, the observed broadening is similar in size to the expected effect due to the initial velocities from the zero point motion, which was estimated in Sec. III B. The following analysis therefore concentrates on the v_a distributions, which are sensitive to the most interesting (while long-lived) breathing excitations $(v_1,0^0)$.

The measured v_a distributions were fitted for a number of time slices by superpositions of a smooth function representing the relaxed data [$t > 2$ s according to Fig. 5(a)] plus the Monte-Carlo simulated v_a distributions for the two lowest excited, metastable breathing levels $(1,0^0)$ and $(2,0^0)$ shown in Fig. 1(a). In order to obtain a high sensitivity for small excited-level contributions, it turned out to be important to reproduce all details of the cold data by using an arbitrary smooth function instead of the simulated v_a distribution for the $(0,0^0)$ ground state, which still shows small but statistically significant deviations from the measured relaxed data, hardly visible in Fig. 5(a). Moreover, the population of the $(2,0^0)$ level was fixed to zero in the fits for $t > 600$ ms.

The derived time dependent excited-state populations are plotted in Fig. 6. The earliest time interval for which meaningful state populations could be obtained by this procedure is centered at 30 ms. At this time the population fractions still carried by the $v_1 = 1$ and $v_1 = 2$ states are about 17% and 4%, respectively. It should be pointed out, however, that in contrast to the $v_1 = 1$ fraction, which can be uniquely attributed to the $(1,0^0)$ state at least after the first 100 ms (when it represents essentially all the deviations from the cold data), the $v_1 = 2$ fraction cannot safely be assumed to represent the population of the $(2,0^0)$ state alone, as higher-lying breathing- or even bending-mode excitations may decay with time constants of the same order of magnitude; the statistical accuracy of the data did not allow contributions of higher excited states to be extracted in a meaningful manner. Also shown in Fig. 6 are the exponential decay curves expected when the radiative lifetimes $\tau_{\text{no rot}}$ of 1.18 s and 0.38 s, calculated for the metastable $(1,0^0)$ and $(2,0^0)$ states in the rotationless approximation (c.f. Sec. III A), are assumed to govern the time dependence of the $v = 1$ and 2 populations, respectively. While the long-time behaviour ($t \geq \tau_{\text{no rot}}$) of the measured decay curves seems to be reasonable well represented by these two exponentials, the state specific populations are observed to decay much faster at short times ($t \ll \tau_{\text{no rot}}$). It is interesting now to address these deviations, which lead to effective relaxation times considerably shorter than the radiative lifetimes predicted for the breathing vibrational states in

their rotational ground state.

IV. RO-VIBRATIONAL RELAXATION MODEL

The above results demonstrate that the H_3^+ ions produced under the conditions of the present experiment carry a significant vibrational excitation immediately after leaving the ion source, but that their relaxation to the vibrational ground state is almost complete after $\sim$2 s of storage time. For the breathing mode, the relaxation is slow enough to be followed experimentally; however, the observed relaxation times are found to be considerably shorter when compared to the radiative lifetimes of the relevant vibrational levels calculated in the rotationless approximation. The likely reason for this discrepancy is that neglecting rotational effects is inadequate for the situation of the experiment presented here.

In fact, our studies of the DR process (see Sec. I) using H_3^+ and also D_3^+ ions produced and stored under the same conditions as in the present experiment indicate a sizable internal molecular excitation even after storage times as long as 40 s. Two dimensional fragment imaging following the recombination of the stored molecular ions with low-energy free electrons revealed [21, 22] an average excess energy of about 0.3 eV in the initial state of the DR process, which clearly appears to be introduced by the molecular collision partner. As the present CEI results indicate relaxation to the vibrational ground state, only rotations remain as a source for the excess energy seen in the DR measurements. It is useful to recall that the asymptotic velocity distributions as measured by CEI primarily represent the spatial arrangement of the nuclei in the investigated molecules, which is not significantly influenced even by considerable rotational excitation. On the other hand DR, as opposed to the foil interaction in the CEI target, is an energy conserving process and therefore the final state reflects the rotational as well as the vibrational energy of the interacting molecule.

The excess energies of $\sim$0.3 eV seen in the DR of H_3^+ indicate the population of rotational levels with total angular momenta $J \gtrsim 10$ even in the vibrationally relaxed case ($>$ 2 s storage time) and hence also *during* the vibrational relaxation observed at earlier times. For a more adequate interpretation of the relaxation data from our CEI experiment, we therefore adopt the view that the measured level populations represent only a partial aspect of the complex ro-vibrational relaxation of H_3^+ molecules. Starting from a broad initial level distribution, the relaxation is described by the individual rates of spontaneous radiative transitions between all relevant ro-vibrational levels so that at each time the rotational state populations within the excited vibrational levels and their influence on the effective vibrational relaxation rates can be predicted.

The implementation of such a ro-vibrational relaxation model is made possible by the comprehensive line list for H_3^+ published in Ref. [34]. The states covered by these calculations range up to $\sim$1.8 eV in excitation energy. Energies, total angular momenta and (for many cases) nuclear spin symmetries are given for the tabulated upper and lower levels, together with the spontaneous transition rates between them. This information allows the level populations to be followed as a function of time, but does not yet yield the vibrational relaxation as observed by CEI, as vibrational quantum numbers are not assigned to the listed levels. Fortunately, complete ro-vibrational assignments have been given in a subsequent work [35] for most excited levels up to $\sim$1.2 eV, referring to the same predicted level energies as in Ref. [34]. We have therefore combined the information of Refs. [34, 35] in order to extract the time-dependent populations of all ro-vibrational states assigned to the lowest breathing-excited vibrational levels.

In the model calculations we first extract from the UCL line list [34] all energy levels that appear as lower or upper states, together with their J values and nuclear symmetries which define the statistical weights. Initial populations are then chosen according to a Boltzmann distribution for a given temperature kT_i. The resulting initial population probabilities of the ro-vibrational levels as a function of the excitation energy, assuming an initial temperature of $kT_i = 0.23$ eV, are represented by the light-shaded area in Fig. 7(a). All the $\sim$2500 individual levels with energies up to 12000 cm^{-1} figuring in the UCL line list have been included in this distribution. In addition, based on the assignments from Table I of Ref. [35], the levels belonging to the three lowest breathing-excited levels $(1,0^0)$, $(1,1^1)$ and $(2,0^0)$ could be identified; the resulting populations for the $v_1 = 1$ states and the $v_1 = 2$ state, respectively, are represented by the two areas shown in darker shadings in Fig. 7(a). Assignments are available for all states with $J \leq 12$ and with excitation energies of $\leq$9000 cm^{-1}, as well as for some of the higher lying states. Up to temperatures of $kT_i \sim 0.25$ eV this coverage is large enough to identify a large part of the relevant rotational states within the $(1,0^0)$ and $(1,1^1)$ levels; also the rotational states within the $(2,0^0)$ level are still reasonably represented, although the unaccounted fraction is already increasing. We take the population integrated over all identified states to approximate the total population in a given vibrational level. At $kT_i = 0.23$ eV the total initial population amounts to 14% for the breathing-excited levels $(1,0^0)$ and $(1,1^1)$ (i.e., $v_1 = 1$) and to 1.6% for the $(2,0^0)$ level.

The time dependence of the ro-vibrational state populations is obtained by combining the spontaneous decay rates for the tabulated $\sim$245,000 transitions in a linear rate equation. Examples for the resulting population distributions including *all* ro-vibational states are represented by the light-shaded areas in Fig. 7(b)–(d) for three different storage times; the areas shown in darker shadings represent again the identified contributions of the breathing-excited levels with $v_1 = 1$ and 2. Note that contributions from bending mode excitations have largely

decayed already during the first few milliseconds, leaving only the metastable breathing excitations. In particular, for storage times $\geq$10 ms the $(1,0^0)$ level alone represents essentially the total $v_1 = 1$ population, as the bending-excited level $(1,1^1)$, decaying very fast to the $(1,0^0)$ level, at later times plays only a minor role as an intermediate state in the decay cascade of metastable states with $v_1 \geq 2$. One of the most important results that follow from our model calculations exemplified in Fig. 7 concerns the quasi-stability of the rotational energy tied up in vibrationally relaxed H_3^+ ions over long storage times. While a rotational excitation is found to speed up the decay of vibrationally excited states, many high-lying rotational states built on the vibrational ground state of H_3^+ are still populated after 10 s [see Fig. 7(c)], when even the metastable breathing levels are no longer excited, and any further changes of the population distribution occur very slowly. For the inital condition chosen in the calculations displayed in Fig. 7 the average energy stored in the rotation of the H_3^+ ion after 10 s still amounts to $\langle E_{\rm rot}\rangle = 0.30$ eV and reduces further only to 0.28 eV after 60 s. The quasi-stability and the size of this rotational excitation are consistent with the excitation conditions we were forced to assume to understand our earlier DR-experiments on H_3^+ after storage times of several seconds [21, 22], and motivate our choice of $kT_i = 0.23$ eV for the initial temperature in our model calculations.

The detailed time dependences of the fractional population residing in the breathing levels with $v_1 = 1$ [essentially the $(1,0^0)$ level as discussed above] and in $v_1 = 2$ [as modeled by the $(2,0^0)$ level] were followed in small time steps and the results are shown by the full lines in Fig. 6(a) and (b). For the $v_1 = 1$ states [Fig. 6(a)] our model predicts a rapid decay within the first 500 ms of a substantial part of the population; it proceeds considerably faster than given by the decay time of the rotational ground state of the $(1,0^0)$ level, but approaches the time dependence expected for this state at longer storage times. This is in remarkable agreement with the data and even the absolute magnitude of the population is well accounted for. For the second excited level, the ro-vibrational model also predicts an initial component decaying much more rapidly than given by the respective rotationless decay time; however, as seen in Fig. 6(b), the experiment shows an even larger fast-decaying fraction than predicted. The less good agreement of our model calculation with the data assigned to $v_1 = 2$ is not unexpected considering the omission of unassigned highly excited rotational states for the $(2,0^0)$ level as discussed above. Also, recent theoretical studies indicate that the transition intensities of Ref. [34] should lose some of their accuracy above $\sim$10000 cm^{-1}. Finally, in the data of Fig. 6(b) contributions from even higher excited levels will tend to be subsumized under the $v_1 = 2$ population and can indeed be expected to relax even faster than the $(2,0^0)$ states included in our model calculation. Given these constraints of both the model approach and the experiment, the discrepancies seen for the $v_1 = 2$ population can thus be rationalized.

The good agreement of our model calculation with the observed relaxation behaviour for the $(1,0^0)$ excitations gives strong evidence for a substantial quasi-static rotational exciation of the stored, vibrationally relaxed ions. The dependence of the relaxation curve for the $v_1 = 1$ breathing excitation on the initial temperature and thus on the initial overall ro-vibrational excitation of H_3^+ is illustrated in Fig. 8 for $kT_i = 0.23$ eV, 0.1 eV, and 0.05 eV, respectively; as discussed above we unfortunately cannot increase the temperature substantially above $\sim$ 0.25 eV because of the limitation of our model space. Figure 8 clearly shows that neither the time dependence nor the magnitude of the observed $v_1 = 1$ population can be explained assuming initial temperatures below $\sim$ 0.23 eV. Moreover, the mean energy $\langle E_{\rm rot}\rangle$ expected to be tied up in the rotation of H_3^+ after several seconds of storage amounts, e.g., to only $\sim$ 0.15 eV for $kT_i = 0.1$ eV, too low to be consistent with the mean energy of 0.3 eV observed in the DR measurements [21, 22]. The high initial ro-vibrational excitation required to obtain a consistent picture is not too surprising in view of the source conditions used to produce H_3^+, which involve collisions between H_2 and internally still hot H_2^+ ions produced by electron bombardment and do not allow the H_3^+ molecules formed in these exothermic collisions to relax before their extraction from the plasma. We emphasize, nevertheless, that the use of a thermal (Boltzmann) distribution for the initial level populations is motivated primarily by its simplicity and not by the aim of modeling specific ion source conditions.

The high lying rotational states with energies $\gtrsim$0.5 eV which remain populated for long times [Fig. 7(c), (d)] are associated with states where the axis of rotation is nearly parallel to the C_{3v} symmetry axis (projection quantum number $K \sim J$). States with excitation energies up to 1.2 eV are populated even after 60 s of storage. Remarkably, the recombination imaging experiments on H_3^+ [21, 22] mentioned above indicate also the presence of DR events via the additional dissociation channel $H_3^+(v,J) + e \rightarrow H(n=2) + H_2$ [cf. Eq. (1)], which needs initial state energies exceeding the threshold energy of 0.96 eV. These reactions could indeed become possible by the quasi-stable population of very high-lying rotational levels. From the ro-vibrational model the relative population of all levels exceeding 0.96 eV would be of the order of 1.1% after 10 s and $\sim$0.9% after 60 s, while the relative signal strength ascribed to the additional dissociation channel amounts to $\sim$5% [22]. These numbers might suggest that the rate coefficient for the described reaction channel, involving high-J H_3^+ ions, is much higher than that for the standard reaction defined by Eq. (1).

V. DISCUSSION AND CONCLUSIONS

The CEI experiments, together with theoretical predictions for the nuclear wavefunctions of low-lying vibrational levels for this molecule, have demonstrated that a beam of H_3^+ ions, produced in a standard plasma source, contains a moderate fraction ($\sim$5–15%) of vibrationally excited species during the first second of storage; however, after storage times exceeding 2 s the ions are found to have completely relaxed to the vibrational ground state by spontaneous radiative transitions. On the other hand, the observed relaxation rates, in comparison with a ro-vibrational relaxation model, indicate that a large fraction of the ions is rotationally excited. From the model, it is also seen that many highly excited rotational states are very long lived. As described in Sec. IV, this yields a consistent interpretation of experiments on the dissociative recombination of H_3^+ ions performed under similar conditions, which gave complementary indications of a strong rotational excitation after many seconds of beam storage.

Accepting the presence of rotational excitation at a degree consistent with the recombination data, the observed decay curve of the population in the lowest metastable vibrational level $(1, 0^0)$ can be well reproduced by theoretical predictions. This presents a valuable experimental confirmation of predicted absolute line intensities and radiative decay rates for the ro-vibrational levels of H_3^+, which are largely untested by observations so far. For the second metastable breathing level $(2, 0^0)$ the agreement is less good, but the unfeasibility to include even higher excited levels in the analysing procedure reduces the accuracy of the experimental data, while the present limit of level assignments also reduces the reliability of the ro-vibrational model for the $(2, 0^0)$ excitation.

One of the most important implications of our results is related to the discrepancies between the different experiments where rate coefficients for the dissociative recombination of H_3^+ have been measured. Based on the results presented here, and on the analysis of the recombination imaging data [21, 22] obtained under similar storage conditions, it is very likely that previous rate coefficient measurements [17–19] at ion storage rings were performed on rotationally hot molecular ions; recent measurements of this type, employing ion storage times of many seconds, have in fact observed [36] an influence of the ion source conditions (and hence possibly the population of excited rotational states) on the recombination rate coefficient.

Many properties of H_3^+, from the recombination rates with low-energy electrons to the line intensities in vibrational bands, are either suspected or known to depend strongly on the particular rotational state of the molecule. Ultimately, by using cold ion sources and cryogenic traps [37, 38], it can be envisaged to prepare H_3^+ ions in essentially a single rotational level and in particular in its ro-vibrational ground state. The acceleration of ions from such traps and their transfer into a storage ring might then open up the possibility of performing rotational state selective recombination measurements on this important molecular species.

ACKNOWLEDGMENTS

This work has been funded in part by the German Federal Minister for Education, Science, Research and Technology (BMBF) within the framework of the German-Israeli Project Cooperation in Future-Oriented Topics (DIP), and by the European Community's Research Training Networks Programme under contract HPRN-CT-2000-0142, ETR.

REFERENCES

[1] I. R. McNab, Adv. Chem. Phys. **89**, 1 (1995).
[2] J. Tennyson, Rep. Prog. Phys. **57**, 421 (1995).
[3] A. Suzor-Weiner and I. F. Schneider, Nature **412**, 871 (2001).
[4] V. Kokoouline, C. H. Greene, and B. D. Esry, Nature **412**, 891 (2001).
[5] I. Mistrik, R. Reichle, H. Helm, and U. Müller, Phys. Rev. A **63**, 042711 (2001), and references therein.
[6] T. Oka, Philos. Trans. R. Soc. London, Ser. A **358**, 2363 (2000).
[7] E. Herbst and W. Klemperer, Astrophys. J. **185**, 505 (1973).
[8] A. Dalgarno, Adv. At. Mol. Opt. Phys. **32**, 57 (1994).
[9] T. R. Geballe and T. Oka, Nature **384**, 334 (1996).
[10] B. J. McCall, T. R. Geballe, K. H. Hinkle, and T. Oka, Science **279**, 1910 (1998).
[11] S. Datz, G. Sundström, C. Biedermann, L. Broström, H. Danared, S. Mannervik, J. R. Mowat, and M. Larsson, Phys. Rev. Lett. **74**, 896 (1995).
[12] G. P. des Forets and E. Roueff, Philos. Trans. R. Soc. London, Ser. A **358**, 2549 (2000).
[13] M. Larsson, Philos. Trans. R. Soc. London, Ser. A **358**, 2441 (2000).
[14] M. Larsson, Annu. Rev. Phys. Chem. **48**, 151 (1997).
[15] Z. Amitay, A. Baer, M. Dahan, J. Levin, Z. Vager, D. Zajfman, L. Knoll, M. Lange, D. Schwalm, R. Wester, et al., Phys. Rev. A **60**, 3769 (1999).
[16] U. Hechtfischer, Z. Amitay, P. Forck, J. L. M. Lange, M. Schmitt, U. Schramm, D. Schwalm, R. Wester, D. Zajfman, and A. Wolf, Phys. Rev. Lett. **80**, 2809 (1998).
[17] M. Larsson, H. Danared, J. R. Mowat, P. Sigray, G. Sundström, L. Broström, A. Filevich, A. Källberg, S. Mannervik, K. G. Rensfelt, et al., Phys. Rev. Lett. **70**, 430 (1993).

[18] T. Tanabe, in *Dissociative Recombination: Theory, Experiment and Applications IV*, edited by M. Larsson, J. B. A. Mitchell, and I. F. Schneider (World Scientific, Singapore, 2000), pp. 170–179.
[19] M. Jensen, H. Pedersen, C. Safvan, K. Seiersen, X. Urbain, and L. Andersen, Phys. Rev A. **63**, 052701 (2001).
[20] B. J. McCall and T. Oka, Science **287**, 5460 (2000).
[21] D. Strasser, L. Lammich, S. Krohn, M. Lange, H. Kreckel, J. Levin, D. Schwalm, Z. Vager, R. Wester, A. Wolf, et al., Phys. Rev. Lett. **86**, 779 (2001).
[22] D. Strasser, L. Lammich, H. Kreckel, S. Krohn, M. Lange, A. Naaman, D. Schwalm, A. Wolf, and D. Zajfman, submitted to Phys. Rev. A.
[23] Z. Vager, R. Naamann, and E. P. Kanter, Science **244**, 426 (1989).
[24] Z. Amitay, A. Baer, M. Dahan, L. Knoll, J. Levin, I. F. Schneider, D. Schwalm, A. Suzor-Weiner, Z. Vager, R. Wester, et al., Science **281**, 5373 (1998).
[25] S. Krohn, Z. Amitay, A. Baer, J. Levin, D. Zajfman, M. Lange, L. Knoll, D. Schwalm, R. Wester, and A. Wolf, Phys. Rev. A **62**, 032713 (2000).
[26] R. Wester, F. Albrecht, M. Grieser, L. Knoll, R. Repnow, D. Schwalm, A. Wolf, A. Baer, J. Levin, Z. Vager, et al., Nucl. Instrum. Methods A **413**, 379 (1998).
[27] J. Levin, L. Knoll, M. Scheffel, D. Schwalm, R. Wester, A. Wolf, A. Baer, Z. Vager, D. Zajfman, and V. K. Liechtenstein, Nucl. Instrum. Methods B **168**, 268 (2000).
[28] M. Scheffel, Diploma thesis, University of Heidelberg, 1999.
[29] B. M. Dinelli, S. Miller, and J. Tennyson, J. Mol. Spectrosc. **153**, 778 (1992); Einstein A coefficients were taken from the revised Table II in the Erratum, J. Mol. Spectrosc. **156**, 243 (1992).
[30] F.-S. Pan and T. Oka, Astrophys. J. **305**, 518 (1986).
[31] D. Zajfman, T. Graber, E. P. Kanter, and Z. Vager, Phys. Rev. A **46**, 194 (1992).
[32] J. Tennyson, J. R. Henderson, and N. G. Fulton, Comp. Phys. Commun. **86**, 175 (1995).
[33] O. L. Polyansky and J. Tennyson, J. Chem. Phys. **110**, 5056 (1999).
[34] L. Neale, S. Miller, and J. Tennyson, Astrophys. J. **464**, 516 (1996).
[35] B. M. Dinelli, L. Neale, O. L. Polyansky, and J. Tennyson, J. Mol. Spectrosc. **181**, 142 (1997).
[36] M. Larsson (private communication).
[37] D. Gerlich, Adv. Chem. Phys. **82**, 1 (1992).
[38] D. Gerlich, Physica Scripta **T59**, 256 (1995).

FIGURES

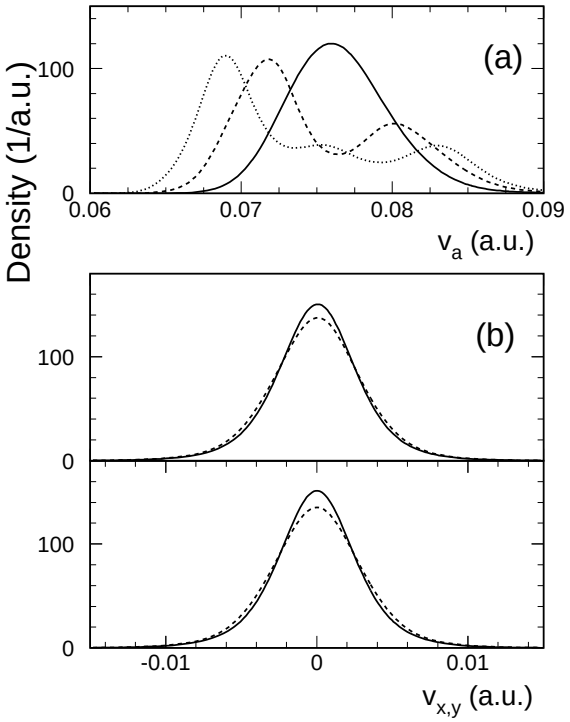

FIG. 1: Simulated asymptotic velocity distributions (normalized) for (a) the breathing coordinate v_a and the ground state $(0,0^0)$ (solid line) as well as the lowest breathing-excited levels $(1,0^0)$ (dashed line) and $(2,0^0)$ (dotted line), and for (b) the bending coordinates $v_{x,y}$ and the ground state $(0,0^0)$ (solid lines) as well as the lowest bending-excited level $(0,1^1)$ (dashed lines). The underlying wave functions were all calculated in rotationless approximation. A carbon target of $0.7\,\mu\mathrm{g/cm}^2$ was assumed in the simulation. In the combined graphs for the bending coordinates, here and below, the upper (lower) frame refers to x (y), respectively.

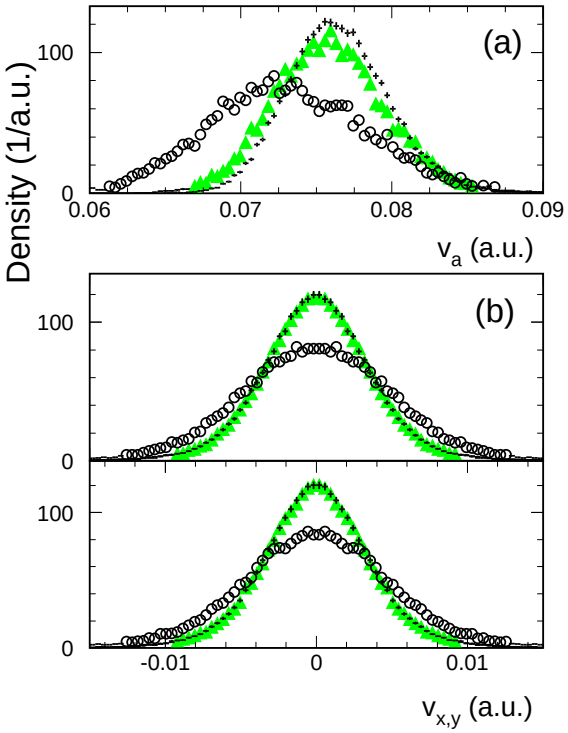

FIG. 2: Asymptotic velocity distributions (normalized) for (a) the breathing coordinate v_a and (b) the bending coordinates v_x, v_y as measured directly after acceleration of the H_3^+ beam (open circles) and after storage times of 30–50 ms (shaded triangles) and > 2 s (crosses).

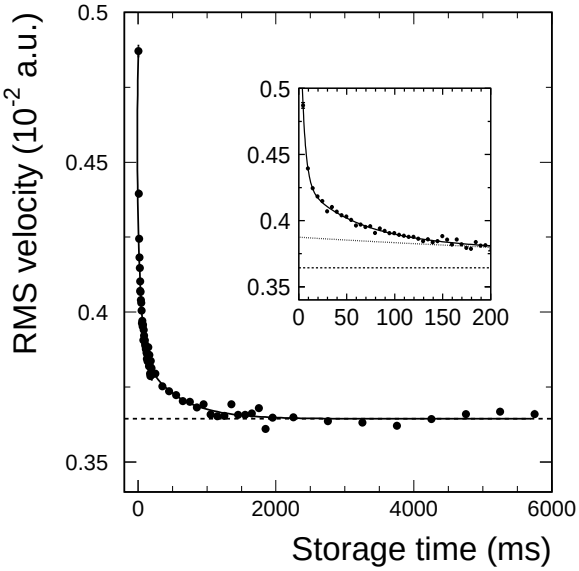

FIG. 3: Root-mean-square width of the v_a distribution as a function of the storage time with a fitted three-component exponential (resulting time constants 500±60, 53±6 and 4.0±0.5 ms). The short-time behaviour (inset) clearly shows the influence of two shorter time constants beside the long-lived component of 500 ms (dotted line). The relaxed r.m.s. velocity is shown by a dashed line.

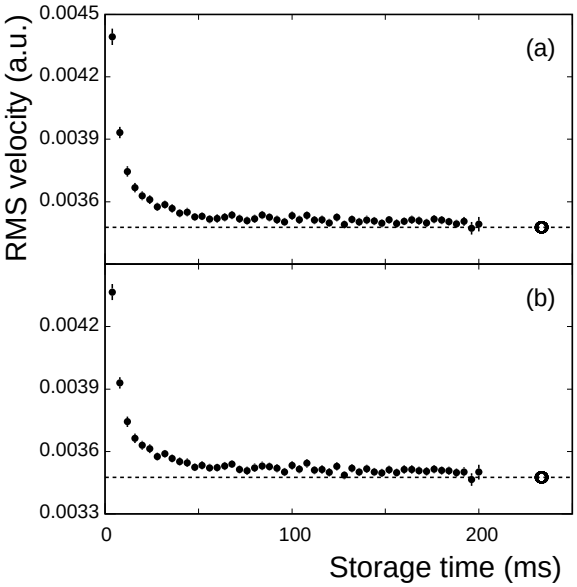

FIG. 4: Root-mean-square width derived from the velocity distributions of the asymetric coordinates v_x (a) and v_y (b) for different storage time intervals up to 200 ms. The relaxed r.m.s. widths of the distribution observed for storage times between 2 and 6 s are shown by the open circles and the dashed lines.

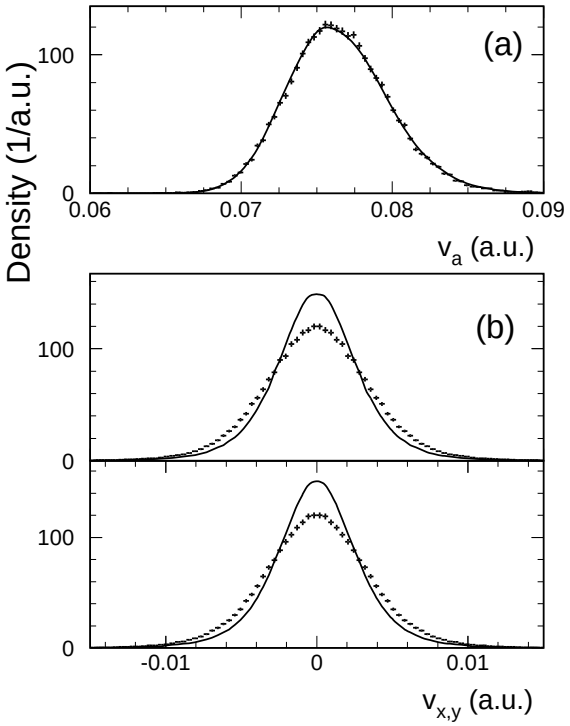

FIG. 5: Asymptotic velocity distributions (normalized) for (a) the breathing coordinate v_a and (b) the bending coordinates v_x, v_y using data for storage times > 2 s (crosses), compared to simulated distributions (full lines).

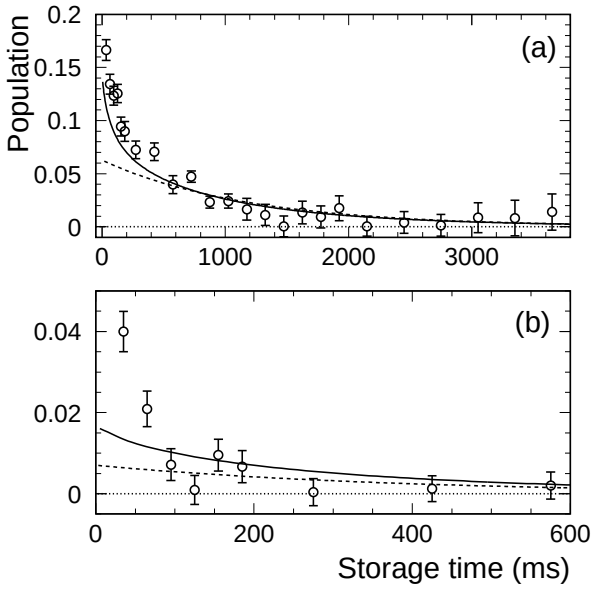

FIG. 6: Population fractions for (a) the first excited breathing level $(1,0^0)$ and (b) the second level $(2,0^0)$, obtained by fitting superpositions of the simulated distributions from Fig. 1(a) to the measured v_a velocity distributions for storage time bins centered at the indicated data points. The dashed lines show single-component exponentials for the rotationless calculated decay time constants of the $(1,0^0)$ and $(2,0^0)$ levels and a constant scaling factor fitted to the data at $t > 500\,\mathrm{ms}$ for $(1,0^0)$ and $t > 70\,\mathrm{ms}$ for $(2,0^0)$. The full lines are the unscaled results for the $(1,0^0)$ and $(2,0^0)$ populations, respectively, of the ro-vibrational model described in the text (initial temperature 0.23 eV).

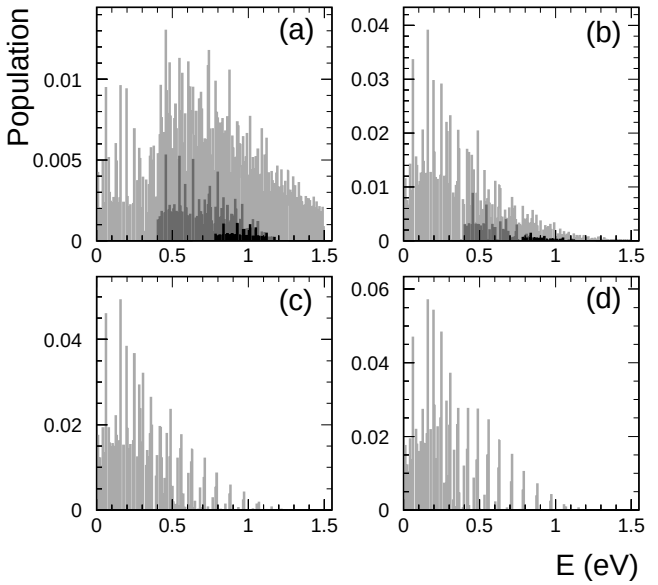

FIG. 7: Ro-vibrational energy distributions (relative populations in $\sim$6.5 meV bins) as obtained for all levels up to 12000 cm^{-1} in the UCL line list (light shaded areas) and for the levels with assigned breathing quantum numbers of $v_1 = 1$ (darker shaded areas) and $v_1 = 2$ (black areas). Initial thermal distribution (a) for a temperature of 0.23 eV; later distributions after 0.1 s (b), 10 s (c) and 60 s (d).

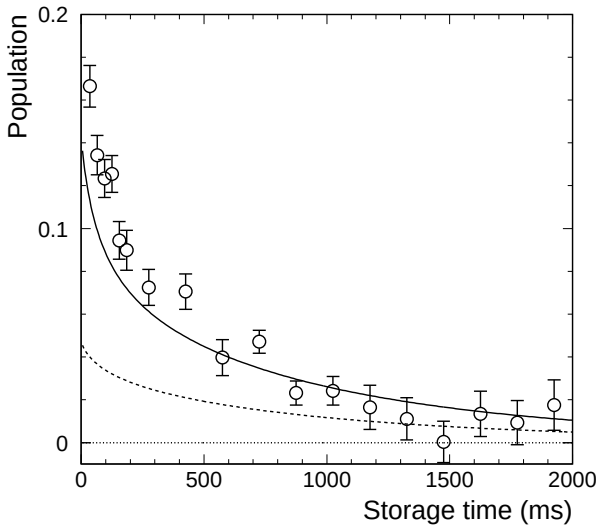

FIG. 8: Early data for the relative population of the first excited breathing level $(1, 0^0)$ [from Fig. 6(a)] compared to the $(1, 0^0)$ populations derived from the ro-vibrational model using initial temperatures of $kT_i = 0.23$ eV (full line) and 0.10 eV (dashed line). At room temperature ($kT_i = 0.025$ eV) the population cannot be distinguished from the zero line in this graph.